Spectrochimica Acta Part A: Molecular and Biomolecular Spectroscopy 275 (2022) 121177

Contents lists available at ScienceDirect

Spectrochimica Acta Part A: Molecular and Biomolecular Spectroscopy

journal homepage: www.elsevier.com/locate/saa

Phycocyanin - carbon dots nanoprobe for the ratiometric fluorescence determination of peroxynitrite

Junjun Shao [a], Shuai Sun [a,b], Da Zhan [b], Lipeng Pan [a], Guangzong Min [a], Xiaobao Li [a], Kailun Huang [a], Wei Chen [a], Likun Yang [a], Xiang-Yang Liu [c], Naibo Lin [a,*]

[a] The Higher Educational Key Laboratory for Biomedical Engineering of Fujian Province, Research Center of Biomedical Engineering of Xiamen, Department of Biomaterials, College of Materials, Xiamen University, 422 Siming Nan Road, Xiamen 361005, People's Republic of China
[b] State Key Laboratory of Luminescence and Applications, Changchun Institute of Optics, Fine Mechanics and Physics, Chinese Academy of Sciences, 3888 Dong Nanhu Road, Changchun 130033, People's Republic of China
[c] State Key Laboratory of Marine Environmental Science, College of Ocean and Earth Sciences, Xiamen University, 422 Siming Nan Road, Xiamen 361005, People's Republic of China

HIGHLIGHTS

- A novel ratiometric fluorescent nanoprobe constructed by Carbon dots and Phycocyanin for determination of peroxynitrite.
- The nanoprobe could sensitively determine peroxynitrite When other reactive oxygen species and interfering substances exist.
- The nanoprobe could accurately determine the content of peroxynitrite in wide range.
- The nanoprobe has preeminent performance including selectivity, wide linear range (0.5–100 μM) and low cytotoxicity.

GRAPHICAL ABSTRACT

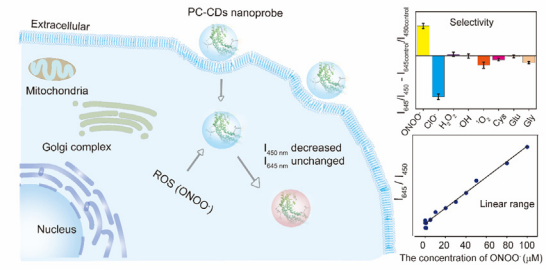

ARTICLE INFO

Article history:
Received 24 January 2022
Received in revised form 14 March 2022
Accepted 17 March 2022
Available online 19 March 2022

Keywords:
Ratiometric nanoprobe
Carbon dots
Reactive oxygen species
Peroxynitrite

ABSTRACT

As a kind of reactive oxygen species, peroxynitrite is related to various diseases closely such as cancer and neurodegenerative diseases. Constructing probes with highly specific ability and a wide linear detection range for peroxynitrite detection is crucial for understanding the pathogenesis of related diseases and optimizing treatments. In this work, we developed a novel luminescent ratiometric fluorescence nanoprobe (PC-CDs) based on carbon dots and phycocyanin. PC-CDs are constructed by amidation reaction between carbon dots and phycocyanin. The nanoprobe we obtained has a good ability of distinguishing peroxynitrite from other reactive oxygen species and interfering substances. Moreover, the linear range of the nanoprobe is 0.5–100 μM and the limit of detection is 0.5 μM when detecting peroxynitrite. In the spiked recovery experiments under phosphate buffered saline (PBS) environment, our nanoprobe has a good recovery performance and the recovery is 99% – 104%, which will be beneficial to the further development of peroxynitrite testing and the research progress of related diseases. Finally, we discuss the quenching mechanism of peroxynitrite for nanoprobe, and found that there is the combination of dynamic and static quenching in the quenching process.

© 2022 Elsevier B.V. All rights reserved.

* Corresponding author.
E-mail address: linnaibo@xmu.edu.cn (N. Lin).

https://doi.org/10.1016/j.saa.2022.121177
1386-1425/© 2022 Elsevier B.V. All rights reserved.

1. Introduction

Reactive oxygen species (ROS) participate in many biology activities and play an important role in regulating various physiological functions in living organisms[1]. Among various ROS, peroxynitrite ($ONOO^-$) is one of highly active ROS (hROS) with strong oxidant properties, which can directly oxidize lipids, proteins and nucleic acids and cause many diseases[2]. The formation of $ONOO^-$ in biology is due to the only known rapid reaction between superoxide anion($O_2^{\cdot -}$) and nitric oxide (NO)[3]. Under pathological conditions, the $ONOO^-$ content in cells is close to 50–100 $\times$ 10^{-6} M min^{-1}, which is much higher than that in normal state (<10^{-6} M min^{-1}) [4]. Besides, due to the very short lifetime of $ONOO^-$, monitoring the content of $ONOO^-$ *in vivo* is very significant for treating related diseases[5].

Fluorescence imaging is known for its excellent temporal and spatial resolution, high sensitivity and non-invasiveness, and has emerged in the detection of $ONOO^-$[6,7]. The fluorescent probes based on small molecule have been widely used for detecting $ONOO^-$, such as boronic ester[8] and methylene blue[9] probes. Many molecule probes are initially nonfluorescent and their fluorescence will turn on through reaction with $ONOO^-$. However, most of the small molecule fluorescent probes used for detecting $ONOO^-$ face challenges such as poor stability, complex synthesis steps and difficulty in resisting environmental changes[10]. Most importantly, they don't have the ability to perform quantitative analysis of $ONOO^-$ in a large concentration range.

Recently, nanoprobes have also been used to detect $ONOO^-$ and are usually very sensitive to detect $ONOO^-$, such as carbon dots (CDs)[11,12], gold nanoclusters[13] and upconversion nanoparticles[14,15]. CDs have emerged in ROS detection because of their stable fluorescence performance[16], simple preparation[16,17], and high biocompatibility[18]. In many reports, CDs have been used to perform qualitative analysis of $ONOO^-$ and show good selectivity [11,19]. However, due to the complex and changeable test environment, accurate quantification of $ONOO^-$ is still a challenge [20].

Most reported nanoprobes based on CDs or other quantum dots used for detecting $ONOO^-$ are single-channel probes[6,11,21]. As we all know, ratiometric fluorescent probes have two fluorescence peaks to reduce the impacts from external environment and internal material changes, and can provide more accurate detections[10]. For the ratiometric nanoprobes of $ONOO^-$, there are still unmet challenges including: small linear range or no linear range[14,22], poor selectivity and low specific recognition ability when other hROS exist in organisms[23,24]. Therefore, it is necessary to construct ratiometric fluorescent probes with high selectivity and wide linear range to improve the quantitative accuracy of $ONOO^-$.

PC has an excellent antioxidant capacity[25] to keep stable fluorescence intensity during the detection of $ONOO^-$. Moreover, PC is a bioactive nutrient with excellent water solubility and biocompatibility[26], and is also a potential drug in clinical applications because of the excellent anti-cancer properties [27]and anti-inflammatory activities[28]. In this work, CDs and PC were linked by amide bonds to build the ratiometric fluorescent nanoprobe (PC-CDs). The nanoprobe not only has a wide linear range (0.5–100 μM), but also exhibits good selectivity for $ONOO^-$. More importantly, we performed $ONOO^-$ quantification experiments in PBS and serum samples and achieved 99%-104% recoveries in the PBS test environment.

2. Experimental

2.1. Materials and reagents

All chemical agents are analytical grade and used directly without further purification. L-glutathione, glycine, citric acid, monohydrate, NaOH, quinine sulfate, glucose and 1-ethyl3 (3-(dimethylamino) propyl) carbodiimide hydrochloride (EDC, 98.0%) were purchased from Aladdin Biochemical Technology Co., Ltd (Shanghai, China). Phycocyanin (PC, lyophilized powder), polyethyleneimine (PEI, 30%) and N-hydroxysulfosuccinimide sodium (NHS, 98.0%) were purchased from Macklin Biochemical Co., Ltd (Shanghai, China). NaClO was purchased from Energy Chemical Co., Ltd (Shanghai, China). $NaNO_2$ was purchased from Sinopharm Chemical Reagent Co., Ltd (Shanghai, China). 30% H_2O_2 and HCl were purchased from Xilong Scientific Co., Ltd (Guangdong, China). Human Serum (9193–50 ml) was purchased from Beijing Lablead Biotech Co., Ltd (Beijing, China).

2.2. Apparatus

The microscopic images of PC-CDs were taken by a transmission electron microscope (TEM, Talos F200s). We confirmed that PC was successfully linked with the CDs by Fourier transform infrared (FTIR, Nicolet is10) spectroscopy. The UV–Vis absorption spectra of CDs and PC-CDs were measured by UV–vis spectrophotometer (UV–Vis, Lambda 750). Fluorescence spectra were determined by a Fluoromax-4 measurement system (HORIBA, JobinYvon. Inc), and the slit for excitation and emission was set to 3 nm. Fluorescence lifetime of CDs and PC-CDs were determined by a FlS980 measurement system (Edinburgh Instruments, UK) with the excitation source of 365 nm. CDs were prepared by a microwave oven (Galanz) at medium to high fire potential.

2.3. Preparation of CDs

CDs were synthesized by a rapid and one-step procedure according to a literature previously reported with some improvements[29]. In short, the CDs were prepared by pyrolyzing citric acid in presence of PEI using a microwave. 1 g citric acid and 0.5 g PEI were added into 20 ml deionized water and then stirred for ten minutes (300 r min^{-1}) to make them dissolve completely. Then, the mixed solution was placed in a microwave and heated for 5 min at medium to high fire potential (700 W). The obtained product was cooled at room temperature for 10 min. The residual impurities were extracted by dialysis cassettes (Solarbio, molecular weight cut-off 8000) for 3 days with deionized water. Finally, CDs were stored at the condition of 4 °C.

2.4. Preparation of PC-CDs

Firstly, 230 μl of PC (1 mg ml^{-1}) solution was added into 4 ml of phosphate buffered saline (PBS, 10 mM, pH = 7.4) buffer, followed by a 720 μl aqueous solution containing 20 mg NHS and 20 mg EDC. Secondly, the mixed solution was then incubated at room temperature for half an hour to activate the carboxyl groups on the PC. Then, 50 μl of CDs (59 mg ml^{-1}) solution was added to the above solution and the mixture was incubated for 24 h at 4 °C. After that, the raw product was purified by dialysis in pure water for 36 h. Finally, PC-CDs were stored at the condition of 4 °C.

2.5. Quantum yield measurements

Quinine sulfate (quantum yield = 0.577) was chosen as a reference standard. The quantum yield of CDs in water is calculated as:$\Phi = \Phi_s(I/I_s)(A_s/A)(n/n_s)^2$. Where Φ is the quantum yield, I is the measured integrated emission intensity, n is the solvent refractive index and A is the optical density. The subscript "s" represents the known relative reference value of the quantum yield.

2.6. Generation of different ROS

Hypochlorite (ClO^-), H_2O_2 stock solutions were delivered from commercial aqueous solutions and the concentrations were determined by their UV–vis absorbance at 292 nm ($\varepsilon = 350M^{-1}cm^{-1}$) and at 240 nm ($\varepsilon = 43.6M^{-1}cm^{-1}$) respectively. Hydroxyl radicals (•OH) was generated by a Fenton reaction, $FeCl_2$ was added in the presence of 10 equiv. of H_2O_2. The concentration of •OH equaled to that of ferrous ion. Singlet oxygen ($^1O_2$) was generated in situ by addition 1 eq. of the H_2O_2 stock solution into a solution containing 10 eq. of HClO. $ONOO^-$ solution was prepared following the reported literature[30]. Briefly, a mixture of $NaNO_2$ (0.6 M) and H_2O_2 (0.7 M) was acidified with HCl (0.6 M), and then NaOH (1.5 M) was added within 1–2 s to make the solution alkaline. The concentration of $ONOO^-$ was determined by the absorbance at 302 nm [$C_{ONOO^-} = Abs_{302nm}/1.67(mM)$].

2.7. General procedure for peroxynitrite detection

Firstly, the concentration of $ONOO^-$ was determined by the UV–vis absorbance at 302 nm [$C_{ONOO^-} = Abs_{302nm}/1.67(mM)$]. Secondly, for detecting $ONOO^-$, various concentrations of $ONOO^-$ (20 μl) were added into the 2 ml PBS buffer solution (10 mM, pH 7.4) containing the PC-CDs with a fixed concentration of 500 μg ml^{-1}. And then, the mixed solutions were incubated at 25 °C for 5 min. Finally, a fluorescence spectrometer was used to measure the emission spectra of these samples at room temperature. For $ONOO^-$ detection in human serum, various concentrations of $ONOO^-$ (50 μl) were added into 50 μl serum. Then, the mixed solutions (20 μl) were added in 2 ml PBS solution (10 mM, pH 7.4) containing the PC-CDs with a fixed concentration of 500 μg ml^{-1}. During testing, there are three parallel samples for each concentration. The fluorescence spectra of all samples were measured under the excitation at 365 nm, and the emission intensities at 450 nm and 645 nm were recorded for quantitative analysis.

2.8. Cytotoxicity assay

MC3T3-E1 cells were cultured in minimum essential medium α (α-MEM) with 10% fetal bovine serum (FBS) and 1% streptomycin-penicillin, which were later incubated at 37 °C in 5% CO_2 atmosphere. Then, 5×10^4 MC3T3-E1 cells were transferred to the 96-well plates (Thermo, USA) containing 100 μl medium and 10 μl CDs or PC-CDs in each well. Cell counting kit-8 (CCK-8) was used to determine cell viability. After seeding the materials for 1, 4, and 7 days, the medium was replaced by 10 μl of CCK-8 solution and 100 μl of fresh medium, then the culture plate was incubated at 37 °C and 5% CO_2 atmosphere for 30–40 min. Optical density (OD) value was detected at 450 nm with a microplate reader (Spectra MAX M2, Molecular Devices, USA).

3. Results and discussion

3.1. Design and characterization of nanoprobe

According to the one-step microwave method[29], CDs were prepared by pyrolyzing of citric acid in the presence of PEI (Fig. 1a). The obtained CDs are featured with blue luminescence under UV excitation light (365 nm) (Fig. S1a). According to the emission spectra at different excitation wavelengths (Fig. S2a), the best excitation for CDs is at 365 nm, and the emission peak is located at 450 nm. Using quinine sulphate as a standard, the fluorescence quantum yield of CDs is calculated to be 37.3%. In addition, the single CDs have a response with $ONOO^-$. The fluorescence intensity of CDs decreases with increasing $ONOO^-$ concentration (Fig. S3a). However, the fluorescence intensity at the wavelength of 450 nm peak has a non-linear relationship with $ONOO^-$ concentration in 0.5–100 μM range (Fig. S3b). As we all know, non-linear relationship is not ideal for quantifying the $ONOO^-$.

To measure $ONOO^-$ precisely, PC was selected as a reference fluorescence to construct the ratiometric probe together with CDs. The CDs were amidated with PC through EDC/NHS to generate nanoparticles (PC-CDs) with a yield of synthesis 78.6%. In addition, the synthesis mechanism is showed in Fig. 1b. From the FT-IR spectra of CDs (Fig. 2d), the spectral band at 3480 cm^{-1} is a result of the N—H stretching vibration. The absorption bands of CDs at 1570 cm^{-1} and 1320 cm^{-1} belongs to amide II and the stretching vibration of C—N bond, respectively. It reveals aminos on the surface of CDs[31]. From the FT-IR spectra of PC, the typical protein bands of amide A, amide I and amide II are observed at 3440 cm^{-1},1660 cm^{-1} and 1560 cm^{-1}, respectively[32]. The spectral bands at 2930 $cm^{-1}$and 2970 cm^{-1} belong to the asymmetric and symmetric stretching vibrations of methylene (–CH_2-), respectively. Compared with native PC, the amide I and amide II bands of the PC-CDs almost remain, which indicates that the characteristic protein structure of PC is not affected and its biological activity still remains after being linked with CDs. In addition, the shift of the characteristic vibration of C—N indicates of CDs indicates the amidation reaction between –NH_2 groups on CDs and –COOH groups on PC. These results prove that CDs have been successfully linked with PC.

Due to a large number of amino groups on the surface of CDs, the zeta potential of CDs is positive. The zeta potential of PC is negative because of the carboxyl groups on the surface. PC-CDs have a lower positive potential, which indicates that CDs are successfully connected to the PC (Fig. 2f). High-resolution transmission electron microscopy (TEM) shows that the average size of PC-CDs is about 25 nm (Fig. S2c). The particles of PC-CDs are uniform, which suggests good dispersibility (Fig. 2a–c). As shown in Fig. 2e, PC-CDs show double emission peaks under 365 nm excitation and the peak positions shift a little compared with individual CDs and PC. It can be attributed to that the changed chemical environment after PC linked with CDs. Based on the emission spectra of PC-CDs under different excitation wavelengths, 365 nm is still selected as the optimal excitation wavelength in our subsequent experiment (Fig. S2b).

3.2. Fluorescence responses with $ONOO^-$

The fluorescence responses of PC-CDs toward $ONOO^-$ are evaluated in PBS solution at room temperature. Fig. 3a shows the representative fluorescence spectra of PC-CDs in the presence of $ONOO^-$. With increasing concentration of $ONOO^-$, the fluorescence intensity of PC-CDs at 450 nm exhibits remarkably quenched, while the fluorescence intensity at 645 nm changes a little. During the experiments, the excitation light we used was 365 nm. The fluorescence peak at 450 nm is derived from CDs, while the fluorescence peak at 645 nm is derived from PC. According to previous reports [11,33], $ONOO^-$ will oxidize the amino groups on the surface of CDs and decline the fluorescence intensity. In addition, the light-absorbing structure of PC will also be oxidized by $ONOO^-$[32]. Therefore, with the addition of $ONOO^-$, both of the fluorescence intensity at 450 nm and 645 nm decrease. However, in our work, the fluorescence intensity at 645 nm decreases only a little, which can be attributed to the competition between PC and CDs. When $ONOO^-$ is added, the absorption capacity of CDs decreases (Fig. 4e). Therefore, PC can absorb more excitation light at 365 nm to enhance the fluorescence intensity at 645 nm. What's more, 365 nm is not the most suitable excitation wavelength for PC (Fig S6a). The destruction of the light-absorbing structure of PC has a limited effect on the fluorescence intensity at 645 nm.

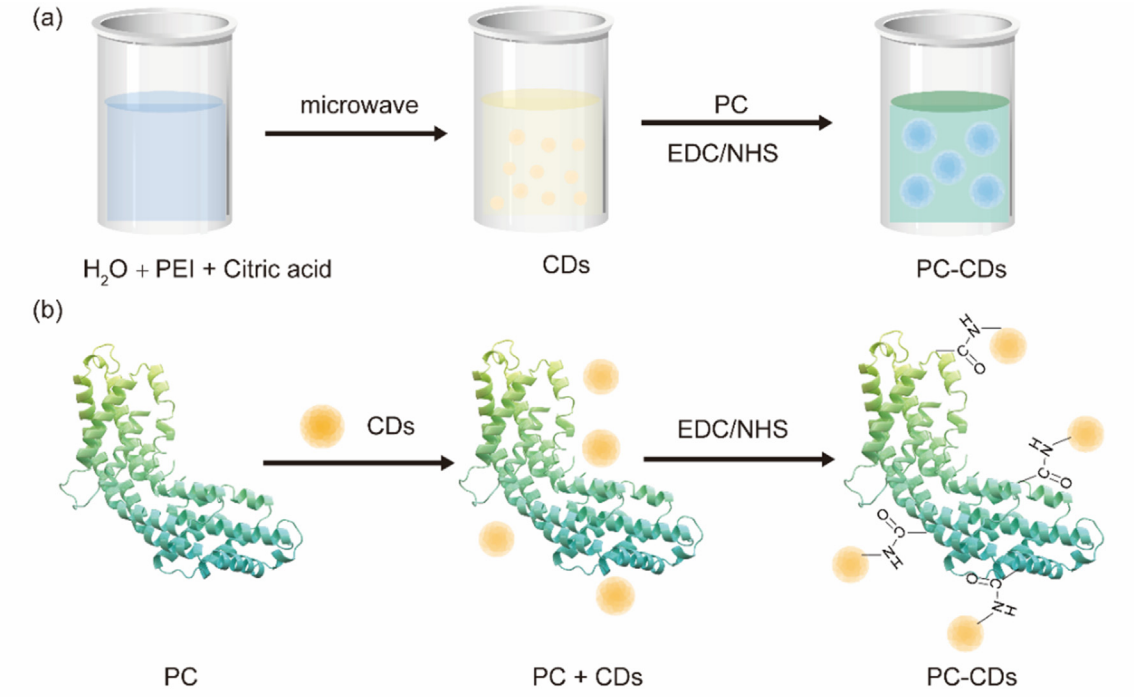

Fig. 1. (a) Synthesis procedures and (b) mechanism of PC-CDs.

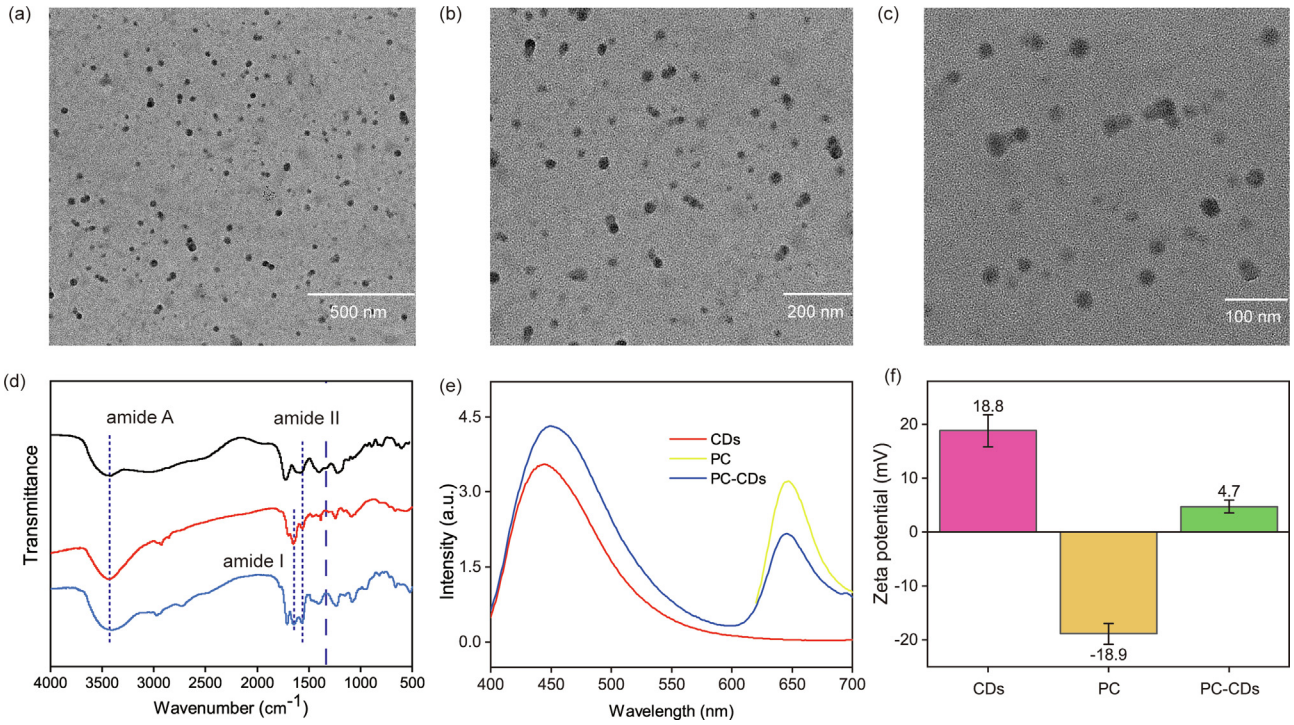

Fig. 2. (a) - (c) TEM images of PC-CDs in different magnifications. (d) FT-IR spectra of PC (red), CDs (black) and PC-CDs (blue). (e) Fluorescence spectra of PC, CDs and PC-CDs under 365 nm excitation. (f) Zeta potentials of PC, CDs and PC-CDs.

Ultimately, the fluorescence intensity at 645 nm changed only a little. Additionally, with the decrease of fluorescence at 450 nm, a clear fluorescence color change from blue to red can be seen under UV light (Fig. S1b and c).From Fig. 3b, the ratiometric fluorescence of PC-CDs (I_{645}/I_{450}) has an excellent linear correlation with the concentration of $ONOO^-$ (0.5–100 μM) and the range is wide enough for pathological conditions (50–100 μM)[4]. The limit of detection of PC-CDs is 0.5 μM. These results mean PC-CDs have a great potential to measure the concentration of $ONOO^-$ accurately in diseases. In addition, other ROS (except ClO^-) and substances without strong oxidizing properties and commonly found in biological matrices such as glucose, have little quenching effect on PC-CDs (Fig. 3c and Fig. S7). It shows that PC-CDs has specificity for $ONOO^-$ when other ROS and interfering substances exist in

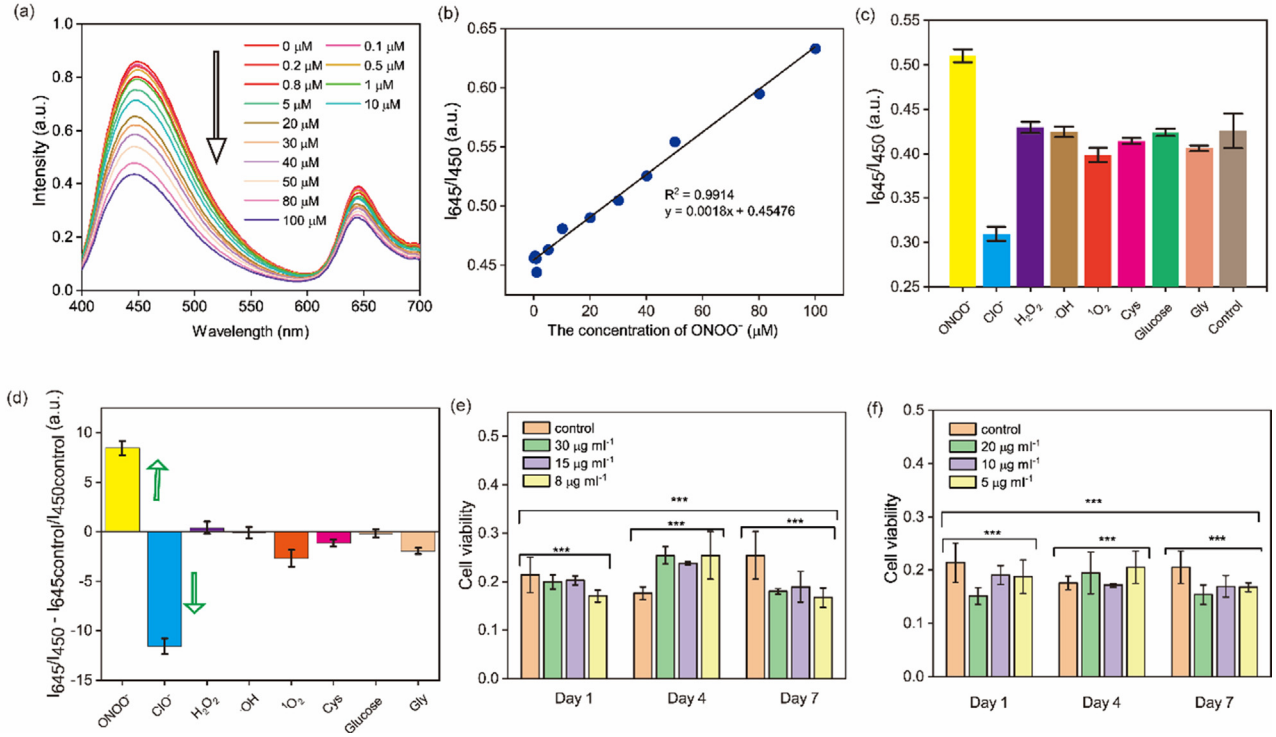

Fig. 3. (a) Fluorescence spectra of PC-CDs with various $ONOO^-$ concentrations. (b) The linearity curve between ratiometric fluorescence and the concentration of $ONOO^-$. (c) Fluorescence responses of PC-CDs toward ROS (30 μM) and different coexistences (1 mM). (d) The changes of fluorescence response ratio compared with the control group ($ONOO^-$). The optical density value at 450 nm of MC3T3-E1 incubated with (e) CDs and (f) PC-CDs for 1, 4, and 7 days. (***, $P < 0.001$).

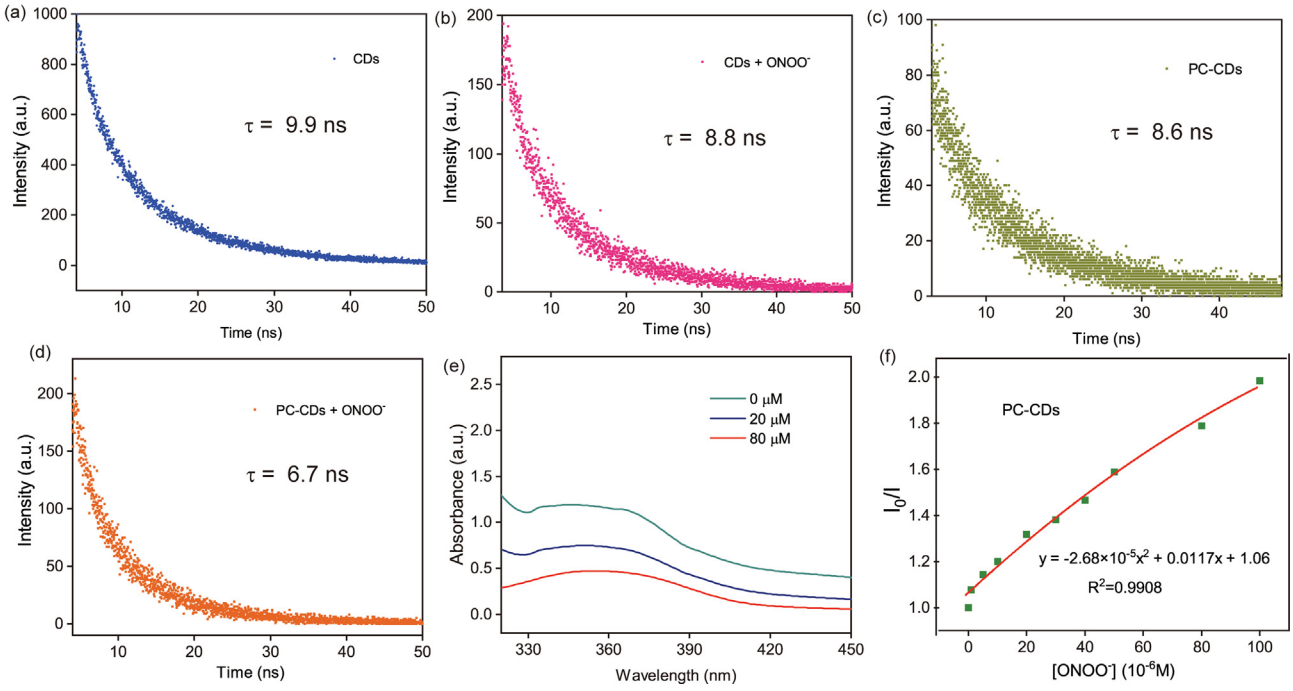

Fig. 4. Fluorescence decay curves of (a) CDs and (c) PC-CDs at 450 nm. Fluorescence decay curves of (b) CDs and (d) PC-CDs with the addition of $ONOO^-$ (30 μM) at 450 nm. (e) Absorption spectra of the CDs (500 μg ml^{-1}) containing various concentrations of $ONOO^-$. (f) Fluorescence intensity ratio (I_0/I) based Stern-Volmer plot.

the tested environment. Interestingly, PC-CDs show the specificity between $ONOO^-$ and ClO^-. As Fig. 3c shows, with the concentration of $ONOO^-$ or ClO^- increasing, the value of I_{645}/I_{450} shows to be greatly different. The fluorescence responses of PC-CDs toward ClO^- are showed in Fig. S4. With increasing ClO^-, the fluorescence intensity at 645 nm and 450 nm all get decreased (especially 645 nm) and the value of I_{645}/I_{450} is getting lower and lower. However, as the concentration of $ONOO^-$ increases, the value of I_{645}/I_{450} is getting larger and larger. This phenomenon can be attributed to the stronger oxidative ability of ClO^- than that of $ONOO^-$. To

demonstrate the distinction brought by ClO^- and $ONOO^-$ more clearly, we took the data processing of subtracting the base value of the control group from other data groups (Fig. 3d). Compared with the control, the ratio increases after adding $ONOO^-$ in PC-CDs and the value (I_{645} / I_{450} − $I_{645\ control}$ / $I_{450\ control}$) is positive. The ratio decreases after adding ClO^- and the value is negative. The different ratios change (I_{645} / I_{450} − $I_{645\ control}$ / $I_{450\ control}$) between ClO^- and $ONOO^-$ can be a standard to differentiate ClO^- and $ONOO^-$. Finally, we achieved the high selectivity of PC-CDs for $ONOO^-$ by the different oxidizing properties of various species and the interaction of $ONOO^-$ with amino groups on the surface of CDs. Compared with the references of ratiometric nanoprobe for $ONOO^-$ detection organized in Table S2, the PC-CDs show a better linear range and selectivity for detecting $ONOO^-$.

3.3. Cytotoxicity assay

To investigate the potential for biological applications, the cytotoxicity test of PC-CDs is necessary. As shown in Fig. 3e and Fig. 3f, compared with the control group, the optical density (OD) values of the cells don't change significantly after culturing the MC3T3-E1 cells with different concentrations of CDs and PC-CDs for 1, 4, and 7 days. This shows that CDs and PC-CDs have little cytotoxicity to cells and exhibit high biocompatibility. Moreover, the OD value of cells treated with CDs and PC-CDs increases on the third day, compared with the control group. This is because CDs and PC-CDs have a response with ROS and consume a little ROS, which will inhibit cell growth.

3.4. Spiked recovery experiments in PBS solutions and serum medium

In some reports[4,20], $ONOO^-$ can be generated from induced cell injury and the concentration of $ONOO^-$ in cells can reach 50 μM and higher. In addition, the concentration of $ONOO^-$ in the patient's serum can reach about 10 μM[34]. To verify the accuracy of PC-CDs, the recovery data with external $ONOO^-$ standard solutions (0–58 μM) to PBS solutions and serum medium (Table 1 and Table S3). We measured the concentration of $ONOO^-$ by ultraviolet spectra. The fluorescence spectra of PC-CDs with different $ONOO^-$ concentrations were obtained in a consistent experimental environment, and the fluorescence intensities at 450 nm and 645 nm were recorded. The measured fluorescence intensity of each concentration will be calculated to get the ratio of I_{645} / I_{450}, and then the ratio is substituted into the equation ($y = 0.0018x + 0.45476$, Fig. 3b) to calculate the corresponding concentrations.

In Table 1, the recovery in PBS is 99% −104%, and the relative standard deviation (RSD) is 0.75% −14%. It indicates that PC-CDs has a good potential to detect $ONOO^-$ in PBS solutions. However, as shown in Table S3, the recovery in serum is 75.7% −88.6%, and the RSD is 2.4% −4.5%. The recovery rate data is not good enough, it may be because the substances in the serum will react with $ONOO^-$, and the concentration of $ONOO^-$ present in the serum is less than we added.

3.5. Mechanism of $ONOO^-$ detection

The fluorescence quenching includes dynamic quenching and static quenching[35-37]. The static quenching process will generate a non-luminescent ground state polymer by the interaction between the fluorescent molecule and quencher. The dynamic quenching process is that the fluorescent molecules collide with the quencher and return from the excited state to the ground state. Firstly, we used the Stern-Volmer plots to analyze the quenching process [11,29]. The quenching of the fluorescence of PC-CDs by $ONOO^-$ was studied at room temperature. As shown in Fig. S5, the quenching process of the fluorescence by $ONOO^-$ can be well fitted with the Stern-Volmer equation ($I_0/I = 1 + K_{SV}[Q] = 1 + K_q\tau_0[Q]$), where I_0 is the initial fluorescence intensity of a fluorophore, I is the fluorescence intensity of the fluorophore after adding a quencher, K_{SV} is the Stern-Volmer constant, $[Q]$ is the concentrations of the quencher, K_q is the quenching constant and τ_0 is the lifetime of the fluorophore without adding the quencher.

In Fig. S5, the plot of I_0/I versus $[Q]$ shows a good linear relationship, which suggests that dynamic quenching exits during the quenching process. During the dynamic quenching process ,the fluorescence lifetime of the fluorescent nanoprobe will be shorten [35]. The changes in fluorescence lifetime in our work have revealed the presence of dynamic quenching (Fig. 4a–d and Table S1). Under the excitation of 365 nm, the fluorescence lifetime of PC-CDs at 450 nm has decreased from 8.6 ns to 6.7 ns after adding $ONOO^-$ (30 μM). The fluorescence lifetime of CDs changes from 9.9 ns to 8.8 ns after adding the quencher ($ONOO^-$). This phenomenon shows that there is dynamic quenching in the quenching process of PC-CDs. Compared with single CDs, the changes of the chemical environment in PC-CDs results in the fluorescence lifetime of PC-CDs is shorter.

However, the value of the bimolecular quenching constant K_q of a quencher in the dynamic quenching process cannot exceed $1 \times 10^{10}\ M^{-1}\ s^{-1}$ in aqueous solution [36]. This value is based on the diffusion rate of oxygen, which is a very effective quencher. When the K_q of a quenching process exceeds this value, it indicates the existence of static quenching. In Fig. S5, K_{sv} = 9180 M^{-1}. According to the previous data, the life time τ_0 = 8.6 ns, the data of K_q can be calculated ($K_q = K_{sv}/\tau_0$) to be $1.067 \times 10^{12}\ M^{-1}\ s^{-1}$. It is so high for $ONOO^-$ whose molecular weight are much higher than oxygen. Thus, it is reasonable to assume that static quenching also exists in the quenching process. Additionally, according to the previous report[37], dynamic quenching affects the excited states of the fluorophores only, and the absorption spectra will not be affected. Therefore, detecting the absorption spectrum of a fluorophore is a good way to judge the presence of static quenching. From Fig. 4e and Fig. S6b, after adding different concentrations of quencher ($ONOO^-$), the absorption spectra of CDs and PC-CDs change a lot. This proves that static quenching occurs during the interaction between the PC-CDs and $ONOO^-$.

All of the above shows that the quenching of PC-CDs by $ONOO^-$ belongs to both static and dynamic quenching. When both static and dynamic quenching are present, the following modified Stern-Volmer plot should be used:$I_0/I = 1 + (K_{SV} + K_{SV})[Q] = 1 + K_dK_S[Q]$, where K_d is the dynamic quenching constant, and K_s is the static quenching con-

Table 1
Standard additions and recovery data in PBS solutions.

Sample no.	Peroxynitrite in samples (10^{-6} mol L^{-1})	Peroxynitrite added (10^{-6} mol L^{-1})	Peroxynitrite found (10^{-6} mol L^{-1})	Recovery (%)	RSD (%)
1	0	14.5	14.8	101	14
2	14.5	14.5	30.4	104	2.6
3	14.5	46.6	57.8	99	0.75
4	29	29	57.8	99	0.79

stant[29]. After using this modified equation, a better fit curve was obtained (Fig. 4f).

4. Conclusion

We prepared a biocompatible ratiometric fluorescent nanoprobe based on CDs and PC for the detection of $ONOO^-$. Our nanoprobe has a high selectivity and a large linear range (0.5–100 μM) for $ONOO^-$. The limit of detection of the nanoprobe can reach 0.5 μM. Moreover, we successfully distinguish $ONOO^-$ with other ROS and interfering substances through a ratio comparison. The quenched mechanism of PC-CDs by $ONOO^-$ is revealed to be the combination of dynamic quenching and static quenching through the analysis of Stern-Volmer plots, fluorescence lifetime and ultraviolet spectra. In addition, our nanoprobe has excellent recovery performance in spiking experiments. This work will be possible for opening up new opportunities for distinguish ROS and estimate the $ONOO^-$ flux in human body and revealing the specific work of $ONOO^-$ different from other ROS in the progress of disease, for example, vascular disease.

CRediT authorship contribution statement

Junjun Shao: Conceptualization, Methodology, Investigation, Data curation, Writing – original draft, Writing – review & editing. **Shuai Sun:** Methodology, Writing – review & editing. **Da Zhan:** Writing – review & editing. **Lipeng Pan:** Writing – review & editing. **Guangzong Min:** Writing – review & editing, Visualization. **Xiaobao Li:** Writing – review & editing. **Kailun Huang:** Formal analysis, Writing – review & editing. **Wei Chen:** Formal analysis, Methodology. **Likun Yang:** Writing – review & editing. **Xiang-Yang Liu:** Writing – review & editing. **Naibo Lin:** Conceptualization, Writing – review & editing, Supervision.

Declaration of Competing Interest

The authors declare that they have no known competing financial interests or personal relationships that could have appeared to influence the work reported in this paper.

Acknowledgment

This work was financially supported by the National Natural Science Foundation of China (Grant Nos. 51773171, 12074322), China; Science and Technology Project of Xiamen City (3502Z20183012), China; Science and Technology Planning Project of Guangdong Province (2018B030331001), China; Shenzhen Science and Technology Plan Project (JCYJ20180504170208402), China. The authors also thank the technical supports from Rui Yu, Hao Wang, Xiuming Zhang, Yange Wang and Yun Yang.

Appendix A. Supplementary material

Supplementary data to this article can be found online at https://doi.org/10.1016/j.saa.2022.121177.

References

[1] C. Nathan, A. Cunningham-Bussel, Beyond oxidative stress: an immunologist's guide to reactive oxygen species, Nat. Rev. Immunol. 13 (5) (2013) 349–361.
[2] H. Guo, J.B. Callaway, J.-Y. Ting, Inflammasomes: mechanism of action, role in disease, and therapeutics, Nat. Med. 21 (7) (2015) 677–687.
[3] R. Radi, Peroxynitrite, a stealthy biological oxidant*, J. Biol. Chem. 288 (37) (2013) 26464–26472.
[4] M.N. Alvarez, L. Piacenza, F. Irigoín, G. Peluffo, R. Radi, Macrophage-derived peroxynitrite diffusion and toxicity to trypanosoma cruzi, Arch. Biochem. Biophys. 432 (2) (2004) 222–232.
[5] G. Ferrer-Sueta, R. Radi, Chemical biology of peroxynitrite: kinetics, diffusion, and radicals, ACS Chem. Biol. 4 (2009) 161–177, https://doi.org/10.1074/jbc.R113.47293610.1021/cb800279q.
[6] D. Cheng, Y. Pan, L.u. Wang, Z. Zeng, L. Yuan, X. Zhang, Y.-T. Chang, Selective visualization of the endogenous peroxynitrite in an inflamed mouse model by a mitochondria-targetable two-photon ratiometric fluorescent probe, J. Am. Chem. Soc. 139 (1) (2017) 285–292.
[7] L. Wu, A.C. Sedgwick, X. Sun, S.D. Bull, X.-P. He, T.D. James, Reaction-based fluorescent probes for the detection and imaging of reactive oxygen, nitrogen, and sulfur species, Accounts Chem. Res. 52 (9) (2019) 2582–2597.
[8] B. Dong, X. Song, X. Kong, C. Wang, Y. Tang, Y. Liu, W. Lin, Simultaneous near-infrared and two-photon in vivo imaging of H_2O_2 using a ratiometric fluorescent probe based on the unique oxidative rearrangement of oxonium, Adv. Mater 28 (39) (2016) 8755–8759.
[9] J.-S. Hu, C. Shao, X. Wang, X. Di, X. Xue, Z. Su, J. Zhao, H.-L. Zhu, H.-K. Liu, Y. Qian, Imaging dynamic peroxynitrite fluxes in epileptic brains with a near-infrared fluorescent probe, Adv. Sci. 6 (15) (2019) 1900341.
[10] M.H. Lee, J.S. Kim, J.L. Sessler, Small molecule-based ratiometric fluorescence probes for cations, anions, and biomolecules, Chem. Soc. Rev. 44 (13) (2015) 4185–4191.
[11] X.X. Wu, S. Sun, Y.H. Wang, J.L. Zhu, K. Jiang, Y.M. Leng, Q.H. Shu, H.W. Lin, A fluorescent carbon-dots-based mitochondria-targetable nanoprobe for peroxynitrite sensing in living cells, Biosens Bioelectron. 90 (2017) 501–507, https://doi.org/10.1016/j.bios.2016.10.060.
[12] W. Zhou, S. Dong, Y. Lin, C. Lu, Insights into the role of nanostructure in the sensing properties of carbon nanodots for improved sensitivity to reactive oxygen species in living cells, ChemComm 53 (13) (2017) 2122–2125.
[13] X. Ran, Z. Wang, F. Pu, Z. Liu, J. Ren, X. Qu, Aggregation-induced emission-active Au nanoclusters for ratiometric sensing and bioimaging of highly reactive oxygen species, ChemComm. 55 (100) (2019) 15097–15100.
[14] X. Liu, H. Lai, J. Peng, D. Cheng, X.-B. Zhang, L. Yuan, Chromophore-modified highly selective ratiometric upconversion nanoprobes for detection of ONOO–related hepatotoxicity in vivo, Small 15 (43) (2019) 1902737.
[15] J.J. Peng, A. Samanta, X. Zeng, S.Y. Han, L. Wang, D.D. Su, D.T.B. Loong, N.Y. Kang, S.J. Park, A.H. All, et al., Real-time in vivo hepatotoxicity monitoring through chromophore-conjugated photon-upconverting nanoprobes, Angew Chem. Int. Ed. 56 (2017) 4165–4169, https://doi.org/10.1002/anie.201612020.
[16] S.Y. Lim, W. Shen, Z. Gao, Carbon quantum dots and their applications, Chem. Soc. Rev. 44 (1) (2015) 362–381.
[17] S. Baker, G. Baker, Luminescent carbon nanodots: emergent nanolights, Angew. Chem. Int. Ed. 49 (38) (2010) 6726–6744.
[18] X.T. Zheng, A. Ananthanarayanan, K.Q. Luo, P. Chen, Glowing graphene quantum dots and carbon dots: properties, syntheses, and biological applications, Small 11 (14) (2015) 1620–1636.
[19] J. Zhu, S. Sun, K. Jiang, Y. Wang, W. Liu, H. Lin, A highly sensitive and selective fluorimetric probe for intracellular peroxynitrite based on photoinduced electron transfer from ferrocene to carbon dots, Biosens. Bioelectron 97 (2017) 150–156, https://doi.org/10.1016/j.bios.2017.05.054.
[20] E.F.C. Simões, J.C.G.E. da Silva, J.M.M. Leitão, Carbon dots from tryptophan doped glucose for peroxynitrite sensing, Anal. Chim. Acta. 852 (2014) 174–180, https://doi.org/10.1016/j.aca.2014.08.050.
[21] C. Zhang, X. Wang, J. Du, Z. Gu, Y. Zhao, Reactive oxygen species-regulating strategies based on nanomaterials for disease treatment, Adv. Sci. 8 (3) (2021) 2002797.
[22] X. Ai, Z. Wang, H. Cheong, Y. Wang, R. Zhang, J. Lin, Y. Zheng, M. Gao, B. Xing, Multispectral optoacoustic imaging of dynamic redox correlation and pathophysiological progression utilizing upconversion nanoprobes, Nat. Commun. 10 (2019) 1087, https://doi.org/10.1038/s41467-019-09001-7.
[23] T. Chen, Y. Hu, Y. Cen, X. Chu, Y.i. Lu, A dual-emission fluorescent nanocomplex of gold-cluster-decorated silica particles for live cell imaging of highly reactive oxygen species, J. Am. Chem. Soc. 135 (31) (2013) 11595–11602.
[24] Z. Chen, Z. Liu, Z. Li, E. Ju, N. Gao, L. Zhou, J. Ren, X. Qu, Upconversion nanoprobes for efficiently in vitro imaging reactive oxygen species and in vivo diagnosing rheumatoid arthritis, Biomaterials 39 (2015) 15–22, https://doi.org/10.1016/j.biomaterials.2014.10.066.
[25] Y.J. Niu, W.J. Zhou, J. Guo, Z.W. Nie, K.T. Shin, N.H. Kim, W.F. Lv, X.S. Cui, C-phycocyanin protects against mitochondrial dysfunction and oxidative stress in parthenogenetic porcine embryos, Sci. Rep. 7 (2017) 16992, https://doi.org/10.1038/s41598-017-17287-0.
[26] R. Croce, H. van Amerongen, Natural strategies for photosynthetic light harvesting, Nat. Chem. Biol. 10 (7) (2014) 492–501.
[27] G. Liao, B. Gao, Y. Gao, X. Yang, X. Cheng, Y. Ou, Phycocyanin inhibits tumorigenic potential of pancreatic cancer cells: role of apoptosis and autophagy, Sci. Rep. 6 (2016) 34564, https://doi.org/10.1038/srep34564.
[28] A.d.F. Brito, A.S. Silva, C.V.C. de Oliveira, A.A. de Souza, P.B. Ferreira, I.L.L. de Souza, L.C. da Cunha Araujo, G. da Silva Félix, R. de Souza Sampaio, R.L. Tavares, R. de Andrade Pereira, M.M. Neto, B.A. da Silva, Spirulina platensis prevents oxidative stress and inflammation promoted by strength training in rats: dose-response relation study, Sci. Rep. 10 (1) (2020).
[29] A. Salinas-Castillo, M. Ariza-Avidad, C. Pritz, M. Camprubí-Robles, B. Fernández, M.J. Ruedas-Rama, A. Megia-Fernández, A. Lapresta-Fernández, F. Santoyo-Gonzalez, A. Schrott-Fischer, L.F. Capitan-Vallvey, Carbon dots for copper detection with down and upconversion fluorescent properties as excitation sources, ChemComm. 49 (11) (2013) 1103.

[30] Y. Li, X. Xie, X. Yang, M. Li, X. Jiao, Y. Sun, X.u. Wang, B.o. Tang, Two-photon fluorescent probe for revealing drug-induced hepatotoxicity via mapping fluctuation of peroxynitrite, Chem. Sci. 8 (5) (2017) 4006–4011.
[31] Q. Wu, A. Fang, H. Li, Y. Zhang, S. Yao, Enzymatic-induced upconversion photoinduced electron transfer for sensing tyrosine in human serum, Biosens Bioelectron. 77 (2016) 957–962, https://doi.org/10.1016/j.bios.2015.10.084.
[32] Y.i. You, S. Cheng, L.i. Zhang, Y. Zhu, C. Zhang, Y. Xian, Rational modulation of the luminescence of upconversion nanomaterials with phycocyanin for the sensing and imaging of myeloperoxidase during an inflammatory process, Anal Chem. 92 (7) (2020) 5091–5099.
[33] Y. Bai, Y. Wang, L. Cao, Y. Jiang, Y. Li, H. Zou, L. Zhan, C. Huang, Self-targeting carbon quantum dots for peroxynitrite detection and imaging in live cells, Anal Chem. 93 (49) (2021) 16466–16473.
[34] M.S.M. Al-Nimer, S.A.H. Al-Obaidi, K.S. Al-Dulaimi, Serum nitric oxide and peroxynitrite levels in adult sero-positive rheumatoid arthritis treated with disease modifying antirheumatic drugs: a preliminary report, Turk. J. Med. Sci. 40 (2010) 191–197, https://doi.org/10.3906/sag-0809-32.
[35] J. Kudr, L. Richtera, K. Xhaxhiu, D. Hynek, Z. Heger, O. Zitka, V. Adam, Carbon dots based FRET for the detection of DNA damage, Biosens. Bioelectron. 92 (2017) 133–139, https://doi.org/10.1016/j.bios.2017.01.067.
[36] F. Fang, S. Kanan, H.H. Patterson, C.S. Cronan, A spectrofluorimetric study of the binding of carbofuran, carbaryl, and aldicarb with dissolved organic matter, Anal. Chim. Acta. 373 (2-3) (1998) 139–151.
[37] J.R. Lakowicz, G. Weber, Quenching of fluorescence by oxygen. Probe for structural fluctuations in macromolecules, Biochem. 12 (1973) 4161–4170, https://doi.org/10.1021/bi00745a020.